Molecular beam studies of weak interactions for openshell systems: The ground and lowest excited states of rare gas oxides

Vincenzo Aquilanti, Roberto Candori, and Fernando Pirani

Citation: The Journal of Chemical Physics **89**, 6157 (1988); doi: 10.1063/1.455432
View online: http://dx.doi.org/10.1063/1.455432
View Table of Contents: http://scitation.aip.org/content/aip/journal/jcp/89/10?ver=pdfcov
Published by the AIP Publishing

Molecular beam studies of weak interactions for open-shell systems: The ground and lowest excited states of rare gas oxides

Vincenzo Aquilanti, Roberto Candori, and Fernando Pirani
Dipartimento di Chimica dell'Universitá, 06100 Perugia, Italy

(Received 4 April 1988; accepted 24 July 1988)

Integral cross sections as a function of velocity for scattering of ground state oxygen atoms by the rare gases have been measured at thermal energy. Analysis of atomic sublevels by a Stern–Gerlach magnet allows a control of the relative contribution from different fine structure scattering channels. The results are analyzed using an adiabatic decoupling scheme to derive the interaction as a spherical part and an anisotropic component, from which information is obtained on the six lowest states of the rare gas oxides and on nonadiabatic coupling terms.

I. INTRODUCTION

This and the following[1] paper report recent results obtained in this laboratory on the interaction of open-shell atoms in the ground state with rare gases. The experimental technique exploits magnetic analysis of atomic sublevels and provides insight on the influence of spin–orbit and electronic angular momenta on the long range part of the potential energy curves.

The analysis follows recent advances in the quantum mechanical treatment of P-state atom collisions, which exploits alternative angular momentum coupling schemes and useful decoupling approximations.[2–4]

The knowledge of these interactions is of interest for the understanding of van der Waals forces. Particular attention will be devoted to systematic trends which are emerging on size, strength, and shape of weak interatomic bonds.

The characterization of these interactions is important, for instance, for the role which these systems may play in the development of UV lasers, for all kinetic processes where intramultiplet mixing and polarization phenomena are explicitly observed and also for understanding orientation and alignment in reactive collisions when dominated by anisotropy at long range.

In this context the oxygen rare gases systems are a very interesting case. Some scattering experiments on $O(^3P)$–rare gas systems had already been performed in this laboratory,[5] but the present results, obtained under much improved experimental conditions, supersede the old ones: they confirm previous qualitative conclusions but permit a much more refined analysis.

The experimental technique is discussed in Sec. II, the theoretical framework for the analysis of results is then presented in Sec. III. The results and their analysis are reported in Sec. IV. The information obtained on potential energy surfaces and on nonadiabatic coupling is discussed in Sec. V. Conclusions follow in Sec. VI. Related work on interactions of $O(^3P)$ atoms with hydrogen and methane molecules is reported elsewhere.[6]

II. EXPERIMENTAL

Measurements of absolute integral cross sections for atom–atom collisions in the thermal energy range have been carried out in this laboratory using the experimental arrangement schematized in Fig. 1. This apparatus has been used over the years[7] for the study of the interactions involving H atoms, rare gases, and simple diatomic molecules such as D_2, N_2, O_2. Therefore only the features relevant to this work will be described.

A. The atomic beam and its magnetic analysis

The oxygen atom beam is produced from a microwave discharge in pure oxygen at a pressure of a few Torr. The beam is velocity selected with a resolution of $\sim \pm 5\%$ (full width at half-maximum): Its velocity distribution is found to be nearly Maxwellian and corresponds to a temperature of $\sim 10^3$ K. The target rare gas atoms are confined in the scattering chamber cooled to liquid air temperature (except for Xe). Typical target gas pressure is in the millitorr range. The absolute values of the cross sections have been obtained by an internal calibration procedure based on the determination of gas flow in the scattering chamber and on the absolute values of the He–Ar cross sections reported in Ref. 8. The beam is detected by a quadrupole mass spectrometer kept in a ultrahigh vacuum chamber. Dimensions of slits are indicated in Fig. 1 and other operating conditions are as described elsewhere[5]: They allow sufficient resolution for the measurement of the true quantum integral cross section.

A Stern–Gerlach magnet [Rabi configuration, see Ref. 9(a)] permits the state analysis of oxygen atom beam, which gives information on the atomic levels involved and allows a characterization of the polarization states[9]: This technique has been used in experiments involving nitrogen,[10,11] oxygen,[5(b),11] and fluorine[1,11–13] atoms. The theory of such a technique requires knowledge of the characteristics of the magnetic selector and of the details (slits and beam paths) of the apparatus. The behavior in the magnetic field depends on the effective magnetic moment of the atom, which in turn depends on how the internal angular momenta (e.g., electron spin S and orbital L) couple.[9] For F atoms, a further coupling occurs with nuclear spin, so a full account of the coupling schemes important in the magnetic analysis procedure is given in the following paper. Here for oxygen atoms (Fig. 2) the magnetic analysis shows that a pure beam of ground state ^3P_j atoms can be obtained by microwave discharge in O_2: The atom beam is essentially free of the possible metastable $O(^1D_2)$. The relative population of the j fine structure components of the ground state ^3P, determined by this analysis, is in agreement with that calculated for a Max-

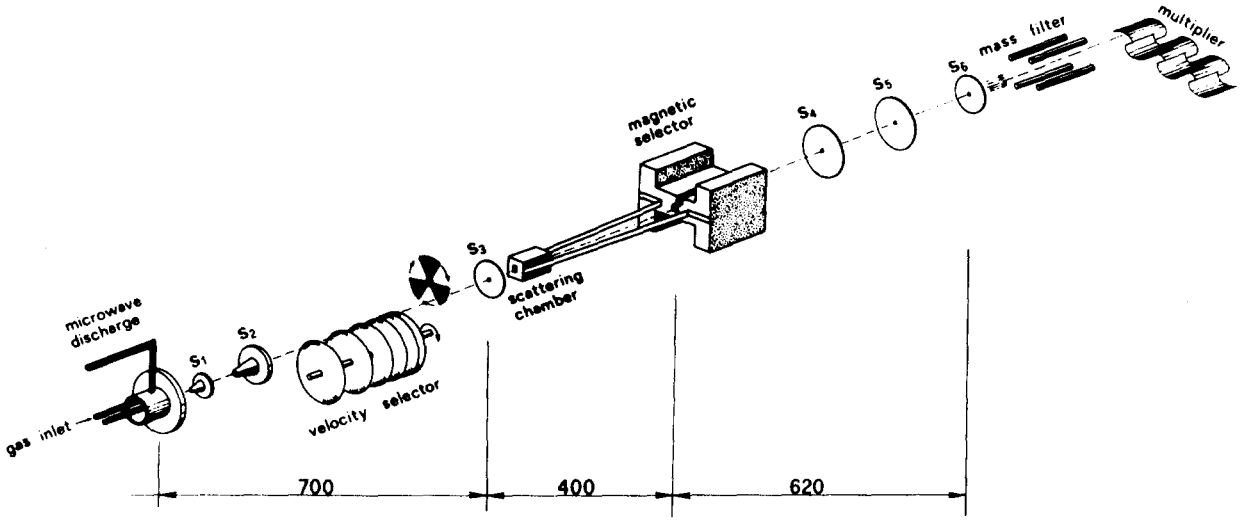

FIG. 1. Schematic view of the apparatus for integral cross section measurements (all dimensions are in mm). The diameter of the collimating slits, which separate differentially pumped chambers, are 1.5 mm for S_1, S_2, S_5, and S_6, 0.7 mm for S_3, and 1.0 mm for S_4.

well–Boltzmann distribution at a beam temperature of 10^3 K (see above). Figure 2 also shows that by varying the magnetic field strength at fixed velocity, it is possible to vary W_{jm_j}, i.e., the relative population of $|jm_j\rangle$ states which are transmitted by the magnetic analyzer [for this treatment, it is taken into account that $j(\mathbf{j} = \mathbf{L} + \mathbf{S})$ is a good quantum number for oxygen atoms in this range of magnetic fields, and m_j refers to the beam direction[14]]. Specifically, for $O(^3P_j)$, the electronic angular momentum $L = 1$,and electronic spin $S = 1$ add to $j = 0$, 1, 2. Therefore, the use of magnetic selection allows to perform cross section measurements with different sublevel populations.

In order that the atoms remain oriented from the collision zone to the stronger inhomogeneous field where magnetic analysis takes place, a weak field which is homogeneous across the beam direction is applied by connecting at the magnet poles two bars of a permeable materials (Fig. 1). These bars extend to embrace the scattering chamber, where the magnetic field was measured to be of the order of 10–50 G. This small field can be shown to be sufficient to avoid spontaneous transitions between the components of atomic magnetic sublevels (Majorana flops).[9]

B. Procedure

Since integral cross sections are obtained from measurements of beam intensities with and without target gas in the scattering chamber, fluctuations and/or drifting of the general experimental conditions in the various part of the apparatus during the measurements, such as vacuum pump operation, electronic circuity and, in particular, microwave discharge parameters, can cause significant random errors. To improve over previous measurements,[5] the target gas is admitted continuously in the scattering chamber under flow conditions calibrated to reach the proper target gas pressure ($\sim 10^{-3} - 10^{-4}$ Torr) and the chamber can be emptied to background pressure (10^{-6} Torr) in less than a second through an additional hole opened by a magnetically operated valve. In this way a whole cycle of measurement is of the order of 20 s. Therefore the measurement time is greatly reduced with respect to previous operating conditions,[5] and a significant improvement in the quality of the scattering data has been achieved. In particular, cross section measurements involving O atoms can be performed with satisfactory accuracy in a wide velocity range even in the presence of a high background mass spectrometric signal at $m/e = 16$.

III. THEORETICAL FRAMEWORK

The theory needed to interpret the experimental results and to obtain information on the interactions has been given and reviewed elsewhere.[2–4,11] At the low collision energy E typical of these experiments, only the fine structure components of the open shell atom are to be included in a close coupling expansion: The multichannel Schrödinger equation at total angular momentum J can be written in a matrix notation

$$\left[-\frac{\hbar^2}{2\mu} \mathbf{1} \frac{d^2}{dR^2} + \mathbf{U}^J(R) \right] \psi = E\psi. \tag{1}$$

In Eq. (1), μ is the reduced mass; the potential energy matrix $\mathbf{U}^J$, which is not diagonal (diabatic representation), is the sum of three contributions:

$$\mathbf{U}^J(R) = \mathbf{V}_{so}(R) + \mathbf{V}_{el}(R) + \mathbf{V}_{rot}(R).$$

The fine structure components are splitted asymptotically by the spin–orbit interaction of the open-shell atom $\mathbf{V}_{so}$; the collision effects are described by the electrostatic interaction between atoms $\mathbf{V}_{el}$, which is relatively short ranged, and by the centrifugal term $\mathbf{V}_{rot}$. These terms have a markedly different dependence on the interatomic distance R: $\mathbf{V}_{so}$ is slowly varying at the long range sampled by our experiments, $\mathbf{V}_{el}$ dies out exponentially, and $\mathbf{V}_{rot}$ decays as R^{-2}. According to the relative importance of these three terms, five alternative representations are possible, corre-

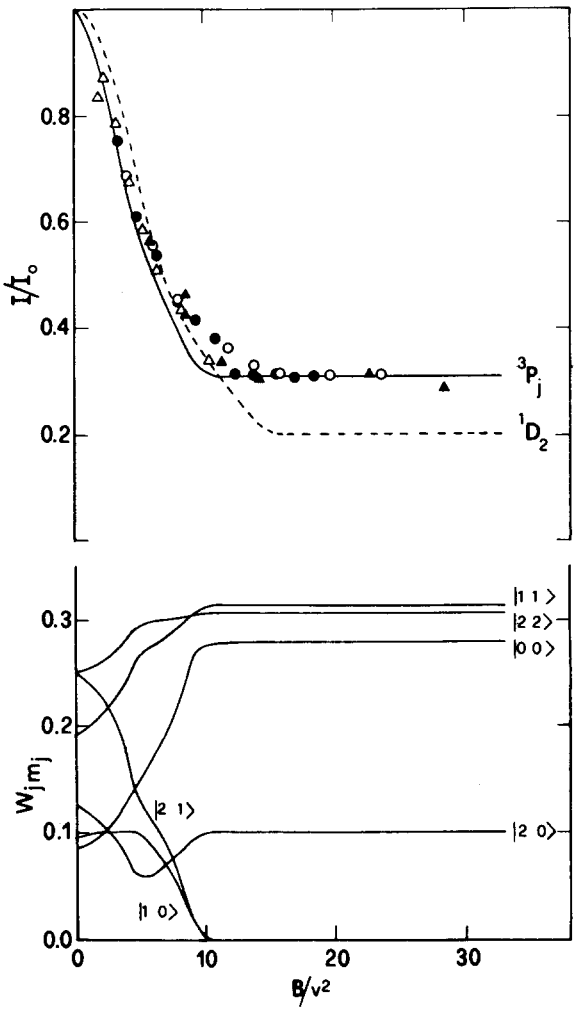

FIG. 2. Fraction I/I_0 of the transmitted oxygen atom beam as a function of the reduced parameter B/v^2, where B is the magnetic induction across the beam and v is the velocity of the atoms. The abscissa units are in 10^2 G km^{-2} s^2. Black triangles, open dots, black dots, open triangles correspond to four different velocities, 1.33, 1.60, 1.80, and 2.21 km s^{-1}. The full line is calculated for the ground ^3P_j state, the dashed line for the metastable $^1D_2$ state. In the lower panel the relative weights W_{jm_j} of the $|j\ m_j\rangle$ states of $O(^3P_j)$ are shown (see also Table I). Atomic $|j\ m_j\rangle$ states under present experimental conditions correlate adiabatically with molecular $|j\ \Omega\rangle$ states (Sec. III).

sponding to different coupling schemes for the angular momenta involved (Hund's cases).

The choice of representations and recipes for simplifications based on decoupling schemes have been given elsewhere.[2,3,11] The simplification considered in the following is justified by the large spin–orbit splitting of the ground state oxygen atom with respect to centrifugal effects. At the relatively small impact parameters relevant for glory scattering, this allows to restrict our attention to only two cases: the molecular case (a) and the diatomic case (c), valid at short and long range, respectively, when the electrostatic interaction is stronger or, respectively, weaker than spin–orbit splitting. A proper label for scattering states is then $|j\ \Omega\rangle$, where j is the atomic angular momentum and Ω is the absolute value of its projection along the R axis.

In this centrifugal sudden or coupled states (CS) decoupling scheme, the Ω quantum numbers is conserved: since at large R Ω tends to the atomic sublevel magnetic projection m_j, the beam direction is the appropriate quantization axis of these experiments[14] and the scattering, which is considered as taking place along adiabatic effective potential curves $V_{|j\,\Omega\rangle}$ is described by the equivalent of Eq. (1) in the adiabatic representation:

$$\left\{-\frac{\hbar^2}{2\mu}\left[\mathbf{1}\frac{d}{dR}+\mathbf{P}(R)\right]^2+\mathbf{V}(R)+\frac{\bar{l}(\bar{l}+1)}{2\mu R^2}\mathbf{1}\right\}\psi=E\psi, \tag{2}$$

where the centrifugal term is approximated by a diagonal centrifugal barrier corresponding to an effective orbital angular momentum $\bar{l}$. This number plays here the role of a parameter, over which for obtaining integral cross sections we will eventually sum until convergence. The effective adiabatic potential curves, which enter into the diagonal matrix $\mathbf{V}(R)$, and the matrix $\mathbf{P}(R)$ of nonadiabatic coupling between them are defined as follows.

In Eq. (2), the diagonal matrix $\mathbf{V}(R)$ contains the eigenvalues of $\mathbf{U}(R)=\mathbf{V}_{el}(R)+\mathbf{V}_{so}(R)$

$$\mathbf{T}(R)\mathbf{U}(R)\tilde{\mathbf{T}}(R)=\mathbf{V}(R). \tag{3}$$

Explicitly in the case of ^3P collisions, in the (c) representation, $\mathbf{U}(R)$ assumes the form[2]

$$\mathbf{U}(R)=\{U^{\Omega}_{JJ'}\}=\begin{bmatrix} U^0_{00} & U^0_{01} & U^0_{02} & & & \\ U^0_{10} & U^0_{11} & U^0_{12} & & 0 & \\ U^0_{20} & U^0_{21} & U^0_{22} & & & \\ & & & U^1_{11} & U^1_{12} & \\ & 0 & & U^1_{21} & U^1_{22} & \\ & & & & & U^2_{22} \end{bmatrix},$$

where

$$U^2_{22}=V_0-\tfrac{1}{5}V_2,$$
$$U^1_{22}=V_0+\tfrac{1}{10}V_2,$$
$$U^1_{21}=U^1_{12}=-\tfrac{3}{10}V_2,$$
$$U^0_{22}=V_0+\tfrac{1}{5}V_2,$$
$$U^0_{20}=U^0_{02}=-\tfrac{\sqrt{2}}{5}V_2,$$
$$U^1_{11}=U^1_{22}+\Delta_1,$$
$$U^0_{11}=U^2_{22}+\Delta_1,$$
$$U^0_{00}=V_0+\Delta_0.$$

Since $U^0_{10}=U^0_{01}=U^0_{21}=U^0_{12}=0$, the upper 3×3 block further block diagonalizes into 1×1 and 2×2 matrices. Here, Δ_1 and Δ_0 are differences between levels of atomic fine structure components, assumed to remain practically constant at the large distances sampled by present experiments. In the case of oxygen $\Delta_1=19.6$ meV, $\Delta_0=28.1$ meV. The potentials V_0 and V_2 are defined by

$$V_0=\frac{2V_{\Pi}+V_{\Sigma}}{3},\quad V_2=\tfrac{5}{3}(V_{\Sigma}-V_{\Pi}).$$

The quantities V_Σ and V_Π are the eigenvalues of electrostatic Hamiltonian $\mathbf{V}_{el}$; they are labeled by the quantum number Λ, the projection of the electronic angular momentum L on the interatomic axis, and, as usual, Σ and Π stand for $\Lambda = 0$ and $\Lambda = 1$, respectively. The spherical part of the interaction V_0 and the anisotropy V_2 are conveniently introduced[2] for the analysis of P atom interactions, extending a suggestion by Reid and Dalgarno.[15]

The elements of the diagonal matrix $\mathbf{V}(R)$ can be obtained from Eq. (3) imposing that

$$\det|\mathbf{U}(R) - \mathbf{V}(R)| = 0.$$

The six solutions of this secular equation are

$$\begin{aligned}
V_{|2\,2\rangle} &= V_0 - \tfrac{1}{5}V_2, \\
V_{|2\,1\rangle} &= V_0 + \tfrac{1}{10}V_2 + \tfrac{1}{2}\Delta_1 - \tfrac{1}{2}(\tfrac{9}{25}V_2^2 + \Delta_1^2)^{1/2}, \\
V_{|2\,0\rangle} &= V_0 + \tfrac{1}{10}V_2 + \tfrac{1}{2}\Delta_0 - \tfrac{1}{2}(\tfrac{9}{25}V_2^2 + \Delta_0^2 - \tfrac{2}{5}\Delta_0 V_2)^{1/2}, \\
V_{|1\,1\rangle} &= V_0 + \tfrac{1}{10}V_2 + \tfrac{1}{2}\Delta_1 + \tfrac{1}{2}(\tfrac{9}{25}V_2^2 + \Delta_1^2)^{1/2}, \\
V_{|1\,0\rangle} &= V_0 - \tfrac{1}{5}V_2 + \Delta_1, \\
V_{|0\,0\rangle} &= V_0 + \tfrac{1}{10}V_2 + \tfrac{1}{2}\Delta_0 + \tfrac{1}{2}(\tfrac{9}{25}V_2^2 + \Delta_0^2 - \tfrac{2}{5}\Delta_0 V_2)^{1/2}.
\end{aligned} \tag{4}$$

These eigenvalues $V_{|j\Omega\rangle}$ are the effective potential energy curves in the adiabatic representation. The coupling between them is represented by the antisymmetric matrix $\mathbf{P}$ which is related to the orthogonal diagonalizing matrix $\mathbf{T}$ appearing in Eq. (3) by

$$\mathbf{P}(R) = \frac{d\mathbf{T}(R)}{dR}\,\tilde{\mathbf{T}}(R).$$

The adiabatic approximation consists in neglecting $\mathbf{P}(R)$ matrix and considering scattering by the six potentials $V_{|j\,\Omega\rangle}$. These adiabatic potentials can be corrected to the first order by putting

$$\mathbf{V}^*(R) = \mathbf{V}(R) - \frac{\hbar^2}{2\mu}\mathbf{P}^2.$$

The term $(\hbar^2/2\mu)\mathbf{P}^2$ represents the correction to the effective potential energy curves in the adiabatic representation due to the coupling between them.

Explicitly, in the case of 2×2 blocks, such as those considered here, $\mathbf{T}$ can be written as a planar rotation

$$\mathbf{T} = \begin{vmatrix} \cos\alpha & \sin\alpha \\ -\sin\alpha & \cos\alpha \end{vmatrix}$$

and

$$\mathbf{P} = \left(\frac{d\alpha}{dR}\right)\begin{vmatrix} 0 & -1 \\ 1 & 0 \end{vmatrix}; \quad \mathbf{P}^2 = -\left(\frac{d\alpha}{dR}\right)^2\mathbf{1},$$

where α represents the rotation angle which describes the transformation from the diabatic to the adiabatic representation.

The elements of $\mathbf{P}$ matrix couple states with different j, but Ω is conserved in this decoupling scheme. Accordingly, they will be indicated as $\langle j\,\Omega|d/dR\,|j'\,\Omega\rangle$ and in the present case are explicitly given by

$$\begin{aligned}
\langle 2\,0|\frac{d}{dR}|0\,0\rangle &= P_{20,00} = \frac{-10/\sqrt{2}}{9\beta_0^2 - 10\beta_0 + 25}\frac{d\beta_0}{dR}, \\
\langle 2\,1|\frac{d}{dR}|1\,1\rangle &= P_{21,11} = \frac{-15/2}{9\beta_1^2 + 25}\frac{d\beta_1}{dR},
\end{aligned} \tag{5}$$

where $\beta_0 \equiv V_2/\Delta_0$ and $\beta_1 \equiv V_2/\Delta_1$.

In this approach, which is similar to the one used also for studying the interaction of fluorine atoms with rare gases,[1] scattering of oxygen atoms is described by the effective adiabatic curves (4), provided that the nonadiabatic coupling between them is negligible. This will be shown below to be the case by explicit computation of the elements of the $\mathbf{P}$ matrix.

This analysis shows that the measured integral cross section can be given by a weighted sum of integral cross sections $Q_{j\Omega}(v)$ for scattering by the potentials $V_{|j\,\Omega\rangle}$:

$$Q(v) = \sum_{j\Omega} W_{j\Omega}\,Q_{j\Omega}(v), \tag{6}$$

where the weights $W_{j\Omega}$, which depend on the magnetic field strength, are known (Fig. 2).

IV. RESULTS AND DATA ANALYSIS

Previous experiments on the scattering of oxygen atoms by the rare gases[5] probed a velocity range where the glory interference effect could be observed for the heavier collision partners. Measurements at relatively high magnetic field strength were carried out for the target gases Ar, Kr, and Xe. Anisotropy effects as measured by differences between cross sections at zero field and at high field, were found to be negligible for Ar, but of the order of a few percent for Kr and for Xe: they showed up in the glory structure of cross sections.

From these data it was inferred that, in the region of the very shallow van der Waals wells of these rare gas oxides, Π-type electrostatic interactions are stronger than Σ ones. The analysis which led to an estimate of the interactions was based on an elastic approximation, as defined in previous papers.[5(b),11] This approximation can only be used for qualitative purposes, but the data did not allow a more quantitative approach.

The present results, obtained under much improved experimental conditions, supersede the old ones and permit a more refined and complete analysis.

Some aspects of O–He results had been communicated recently[16] and in this paper these results have been reanalyzed using the same potential models for V_0 and V_2 as for the other O–rare gas systems, to confirm the systematic trends along the complete series.

The absolute integral cross sections Q for O–He, Ne, Ar, Kr, Xe measured as a function of the beam velocity v are reported in Figs. 3 and 4. In the case of the heavier rare gas systems, the cross sections have been plotted as $Qv^{2/5}$ as customary for exhibiting the glory structure (see Fig. 4). The measurements have been performed, for all systems, at zero and at high magnetic field ($B/v^2 = 1.5$ kG km^{-2} s^2). In Table I the relative population W_{jm_j} of the various $|j\,m_j\rangle$ states present in the beam at zero and at high magnetic field are reported.

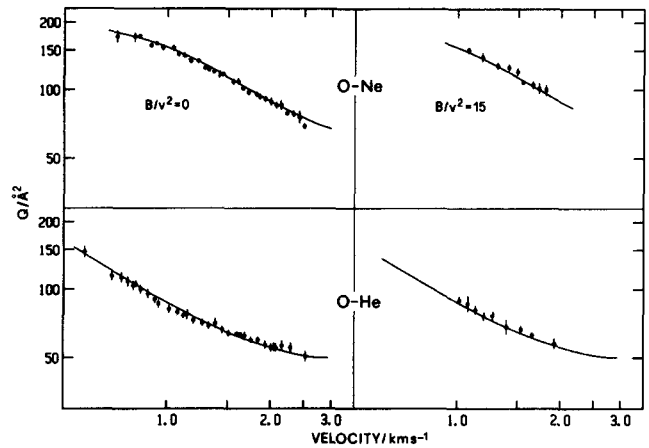

FIG. 3. Absolute integral cross sections for the O–He and O–Ne systems as a function of the velocity v measured at zero (left) and at high (right) magnetic field ($B/v^2 = 15$ in units as in Fig. 2). The curves represent the cross sections calculated according to the procedure described in the text.

In the analysis the cross sections have been calculated using Eq. (6), where the weights $W_{j\Omega}$ are experimentally fixed (see Table I). The integral cross sections $Q_{j\Omega}(v)$ have been obtained by the $V_{|j\,\Omega\rangle}$ potentials using an efficient semiclassical procedure[17] for O–Ar,Kr,Xe and the direct summation of $\bar{l}$-dependent JWKB phases for O–He,Ne. These potentials are generated from Eqs.(4) once V_0 and V_2 are specified.

The experimental results are sufficiently accurate to require a flexible form of the spherical interaction $V_0(R)$. The following Morse–Spline–van der Waals parametrization was used:

$$x = R/R_m; \quad f(x) = V_0(R)/\varepsilon;$$

Morse:

$$f(x) = e^{-2\beta(x-1)} - 2e^{-\beta(x-1)} \quad \text{for } x \leqslant x_1; \tag{7}$$

Spline:

$$f(x) = b_1 + (x - x_1)\{b_2 + (x - x_2)[b_3 + (x - x_1)b_4]\}$$

$$\text{for } x_1 < x < x_2;$$

van der Waals:

$$f(x) = -\left(\frac{C_0}{\epsilon R_m^{\,6}}\right) x^{-6} \quad \text{for } x \geqslant x_2,$$

where C_0 is the long range R^{-6} constant, and ϵ and R_m are the well depth and its location.

For the term $V_2(R) = 5/3(V_\Sigma - V_\Pi)$ the experiments are mainly sensitive to the short range repulsive interactions, which decay exponentially. Simple quantum chemical arguments suggest that in this range $V_\Sigma > V_\Pi$. On the other hand, at long range, $V_\Sigma < V_\Pi$ and $V_2(R)$ is mainly due to the anisotropy in the polarizability of oxygen atom.[18] Therefore, the following, Buckingham-type model has been used:

$$V_2(R) = A_2\, e^{-\alpha_2 R} - C_2/R^{\,6}. \tag{8}$$

The C_0 coefficient in Eq. (7) was obtained from the average velocity dependence of absolute cross sections;[17] the b_1, b_2, b_3, b_4 parameters are automatically fixed by imposing that $f(x)$ have continuous value and derivative both at x_1 and x_2; the C_2 in Eq. (8) was estimated to agree with the anisotropy polarizability of the oxygen atom.[18]

Information on Morse parameters R_m, ϵ, and β, which characterize range, strength and shape of $V_0(R)$, comes mainly from the slope of the cross sections for He and Ne, and from the glory pattern for the heavier rare gases. The anisotropy parameters A_2 and α_2 are related to the overall behavior of cross sections, including the quenching of the glory amplitudes. All these parameters have been varied to obtain the best agreement with the experimental data. The cross sections, calculated in the center of mass frame, have been convoluted to the laboratory system by averaging over the thermal distribution of the target gas in the scattering chamber and taking into account the transmission function of the velocity selector.[19] The potential parameters so obtained are reported in Table II, while the calculated cross sections are compared with those measured in Figs. 3 and 4.

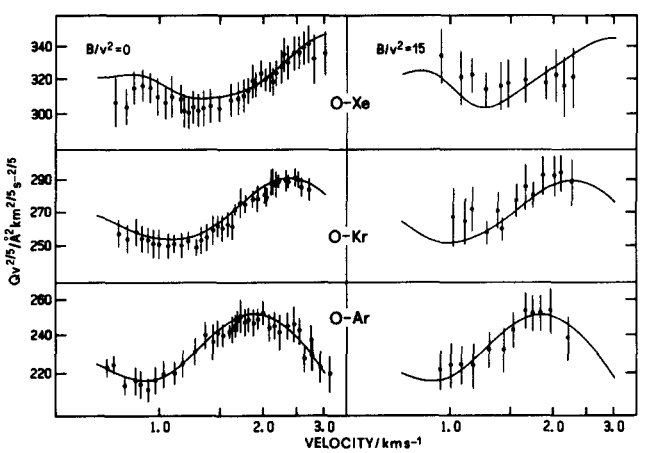

FIG. 4. Absolute integral cross sections for the O–Ar, Kr, and Xe systems as a function of the velocity v measured at zero (left) and at high (right) magnetic field ($B/v^2 = 15$ in units as in Fig. 2). The curves represent the cross sections calculated according to the procedure described in the text.

TABLE I. Relative weights W_{jm_j} of the $|jm_j\rangle$ states of $O(^3P_j)$ at zero and at high magnetic field.[a]

$\|jm_j\rangle$	Zero field	High field
$\|2\,2\rangle$	0.251	0.306
$\|2\,1\rangle$	0.251	0.000
$\|2\,0\rangle$	0.125	0.102
$\|1\,1\rangle$	0.192	0.312
$\|1\,0\rangle$	0.096	0.000
$\|0\,0\rangle$	0.086	0.280

[a]Atomic projections m_j refers to the beam direction. Under present experimental conditions they correlate adiabatically with the projections Ω on the interatomic axis.

TABLE II Potential parameters for the $O(^3P)$–rare gases systems.

Spherical interactions, $V_0(R)$ [Eq.(7)]	O–He	O–Ne	O–Ar	O–Kr	O–Xe
ϵ/meV	2.1	4.3	7.8	9.3	11.8
R_m /Å	3.27	3.30	3.60	3.75	3.90
β	6.5	6.5	6.2	6.2	6.2
C_0/(meV Å^6)	3.482×10^3	7.844×10^3	2.622×10^4	3.870×10^4	6.180×10^4
x_1	1.10	1.12	1.10	1.12	1.10
x_2	1.42	1.50	1.42	1.47	1.42
b_1	−0.7716	−0.7067	−0.7865	−0.7246	−0.7865
b_2	1.8949	1.5362	1.8693	1.6469	1.8894
b_3	−4.2150	−4.4507	−3.7902	−4.1299	−3.7274
b_4	1.4838	4.4784	1.3605	3.2927	0.7030

Anisotropic term, $V_2(R)$ [Eq.(8)]	O–He	O–Ne	O–Ar	O–Kr	O–Xe
A_2/(meV 10^5)	3.4029	1.7204	4.8745	5.7633	8.9994
α_2/Å^{-1}	3.4865	3.1056	2.9298	2.7751	2.7013
C_2/(meV Å^6)	7.659×10^2	1.748×10^3	5.855×10^3	8.546×10^3	1.380×10^4

V. DISCUSSION

In previous sections, the interaction of oxygen atoms with the rare gases was represented by an effective two-body anisotropic interaction, and the anisotropy, at the interatomic distances sampled by these experiments, was mainly attributed to the atomic open shell structure.

Six adiabatic effective potential energy curves correlating with the different atomic sublevels of $O^3(P_j)$ describe this anisotropic interaction. The present analysis gives the curves for O–He, Ne, Ar, Kr, and Xe which are reported in Fig. 5. They are generated using Eq. (4) with the V_0 and V_2 parameters reported in Table II obtained by fitting the present experimental data. Figure 5 shows that main characteristics, such as well depths, their locations, relative separations between curves, change rather regularly from O–He to O–

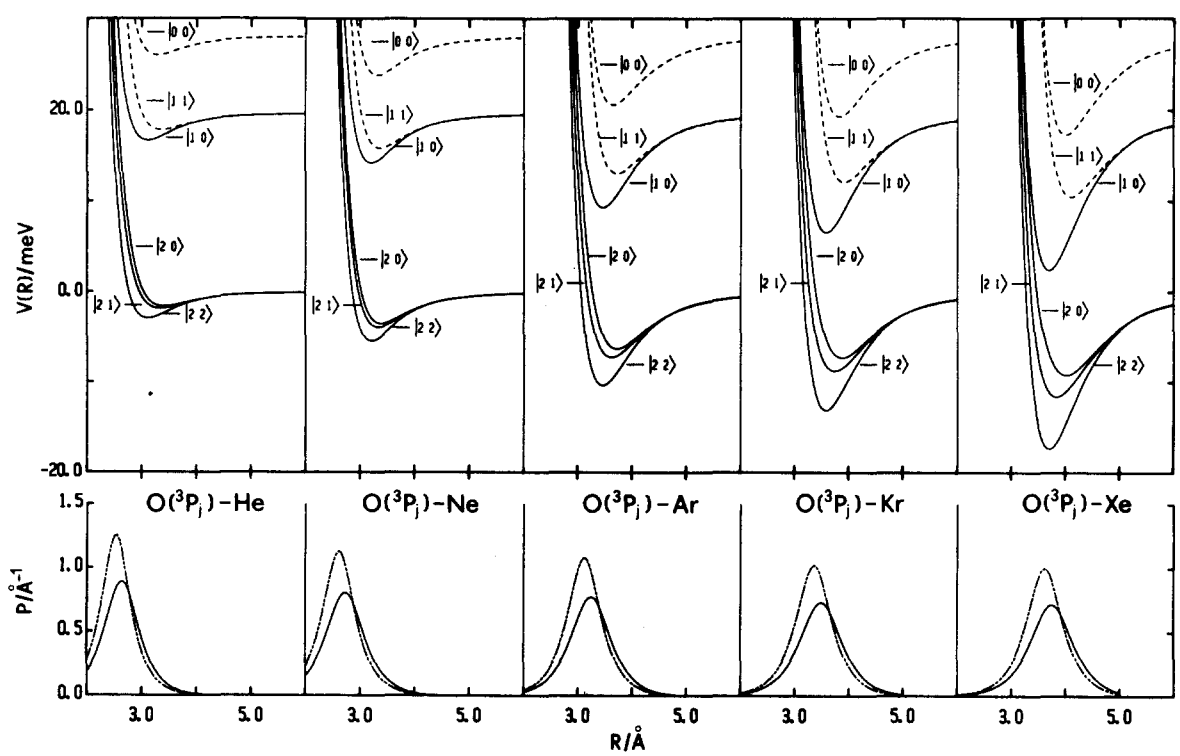

FIG. 5. *Upper panels*: Adiabatic potential energy curves for the $O(^3P_j)$–He, Ne, Ar, Kr, and Xe interactions as obtained from the analysis reported in this work. The curves are labeled using the formalism described in the text. Dashed curves are for Σ symmetry and full curves for Π symmetry. *Lower panels*: Nonadiabatic terms P which couple the $|2\,0\rangle$ and $|0\,0\rangle$ states (dashed curve) and the $|2\,1\rangle$ and $|1\,1\rangle$ states (full curve). Maxima of the P functions mark the separation between coupling schemes, the molecular case (a) at short distances and the diatomic case (c) at long range (see the text).

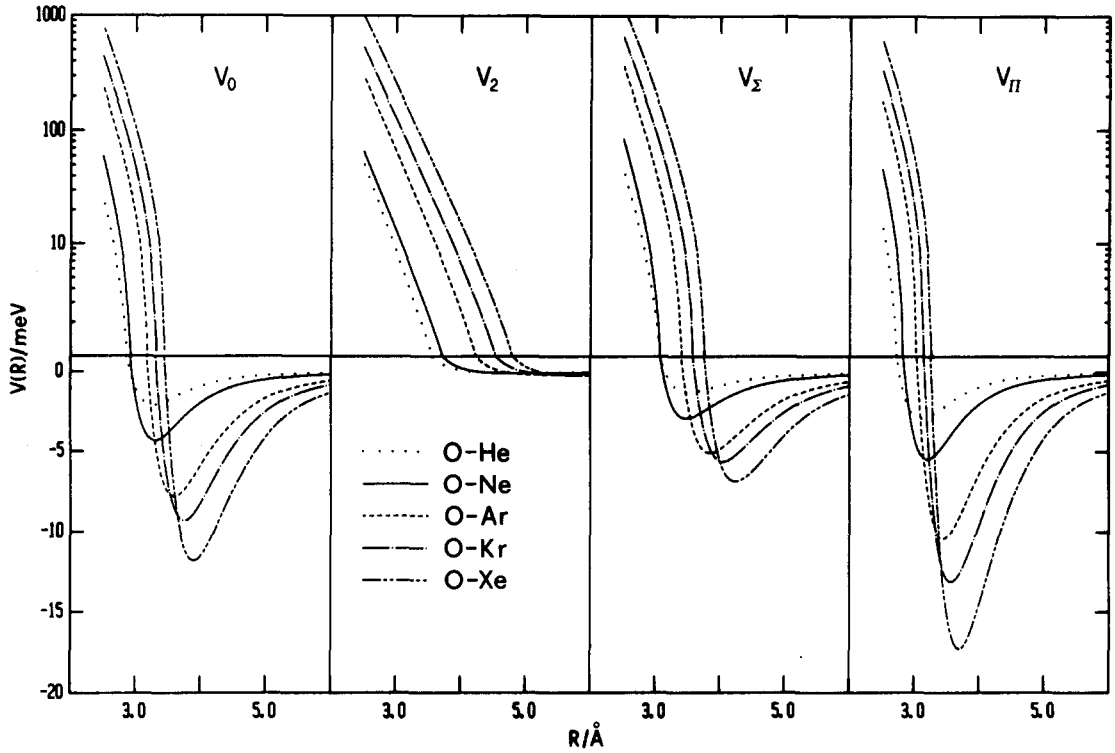

FIG. 6. Comparison between the spherical component V_0, the anisotropic component V_2 and related electrostatic interactions V_Σ and V_Π (see the text) for O–He, Ne, Ar, Kr, and Xe systems.

Xe. A further appreciation of trends comes from a direct comparison of V_0, V_2 and the related interactions V_Σ and V_Π, which are reported for all systems in Fig. 6. Table III lists some relevant parameters for all these potential curves.

TABLE III. Some characteristic features of the O–rare gases interaction.[a]

		O–He	O–Ne	O–Ar	O–Kr	O–Xe
	ϵ	2.1	4.3	7.8	9.3	11.8
V_0	R_m	3.27	3.30	3.60	3.75	3.90
	σ	2.92	2.95	3.20	3.33	3.46
	ϵ	0.05	0.09	0.18	0.17	0.22
V_2	R_m	4.70	4.80	5.21	5.57	5.81
	σ	4.23	4.29	4.66	5.00	5.22
	ϵ	1.3	3.0	5.1	5.6	6.9
V_Σ	R_m	3.52	3.48	3.85	4.05	4.24
	σ	3.15	3.12	3.43	3.61	3.78
	ϵ	3.0	5.5	10.4	13.1	17.3
V_Π	R_m	3.11	3.20	3.45	3.57	3.69
	σ	2.77	2.85	3.05	3.16	3.26
	ϵ	1.9	4.0	7.2	8.8	11.6
$V_{\|21\rangle}$	R_m	3.32	3.33	3.61	3.73	3.81
	σ	2.96	2.96	3.17	3.27	3.35
	ϵ	1.6	3.6	6.3	7.3	9.2
$V_{\|20\rangle}$	R_m	3.40	3.39	3.71	3.86	4.00
	σ	3.03	3.02	3.27	3.38	3.47
	ϵ	1.8	3.8	6.6	7.6	9.3
$V_{\|11\rangle}$	R_m	3.35	3.36	3.71	3.90	4.08
	σ	3.01	3.02	3.32	3.49	3.67
	ϵ	2.1	4.3	7.5	8.8	10.8
$V_{\|00\rangle}$	R_m	3.28	3.31	3.64	3.81	3.99
	σ	2.94	2.97	3.26	3.42	3.60

[a]The parameters for $V_{|22\rangle}$ and for $V_{|10\rangle}$ are the same as for $V_{|1|}$; see Eq. (4). Well depths ϵ, their positions R_m, and zeros of the potentials σ, are in meV and Å, respectively. Estimated uncertainties are about 10% for ϵ and 2% for R_m and σ.

For the V_0 terms both the well depths and their locations increase from O–He to O–Xe, as expected from regularities which are emerging in the present knowledge of the van der Waals forces[20]: In particular, they scale according to the different polarizability of the rare gas atoms. Also the interaction anisotropy appears to increase from He to Xe: Fig. 6 shows that the repulsive walls of the V_2 terms shift towards larger distances from He to Xe, corresponding to an increase in the difference between V_Σ and V_Π potentials. This can be tentatively ascribed to an increasing contribution to the interaction from the excited ionic states, corresponding to a lowering of the ionization potential in going from He to Xe.

Further insight on these interactions is given by the nonadiabatic coupling matrix elements $P(R)$, obtained from Eq. (5) and reported in the lower panels of Fig. 5. The maxima of the $P(R)$ functions mark the transition between an atomic coupling scheme [Hund's case(c)] at long range and a molecular coupling scheme [Hund's case(a)] at short range. They occur when $V_2(R)$ is of the order of fine structure splittings Δ_1 and Δ_0: so, in Fig. 5, the maxima of the two $P(R)$ functions for each O–rare gas system can be seen to be shifted because the $\Omega = 0$ and $\Omega = 1$ coupling terms correspond to different splittings. On the other hand, the maxima for the $\Omega = 0$ matrix elements are higher than those for $\Omega = 1$ because they describe coupling between curves which have a less prominent Σ or Π character.

Table IV reports values and positions of the maxima of the $P(R)$ functions: they are seen to shift at larger distances in going from He to Xe. For O–He the well depths of the interaction involved are described by Hund's case(c) while for O–Xe the maxima of $P(R)$ occur at the distance near the minimum locations. Therefore, the O–Xe system presents a

TABLE IV. Location and values of $P(R)$ function maxima.

		O–He	O–Ne	O–Ar	O–Kr	O–Xe
$P_{20,00}$	$P_{max}/Å^{-1}$	1.25	1.13	1.08	1.03	1.00
	$R_{max}/Å$	2.55	2.60	3.10	3.35	3.60
$P_{21,11}$	$P_{max}/Å^{-1}$	0.89	0.80	0.77	0.73	0.72
	$R_{max}/Å$	2.65	2.75	3.25	3.50	3.75

more prominent molecular character at distances around the energy minima.

The $P(R)$ matrix elements, which are a direct estimate of nonadiabatic effects, are needed to compute intramultiplet mixing, and orientation and alignment cross sections. Finally, as noted in Sec. III, the first order nonadiabatic corrections to the adiabatic curves derived above are $(\hbar^2/2\mu)P^2$ and can be computed to be negligible for all cases, in particular, in the region corresponding to the wells of the interactions probed by these experiments.

VI. CONCLUDING REMARKS

The present investigation has lead to potential functions $V_0(R)$ and $V_2(R)$ which fully characterize the van der Waals forces which bind the diatomic rare gas oxides. Adiabatic curves for the ground and the first few electronic excited states have also been obtained and nonadiabatic coupling terms clearly indicate the angular momentum coupling schemes valid for these molecules in the well regions.

Trends in $V_0(R)$, the spherical part of the interaction, are in agreement with what is presently known on the regularities in van der Waals forces.[20] As noted previously,[16] even for the simplest O–He system, this information has come mainly from scattering studies, because it is still not adequately provided by quantum chemistry, which, however, describes correctly repulsive interactions and features of excited states.[21]

Much less is known on anisotropies in the van der Waals region, and the $V_2(R)$ functions obtained here and in related work on other systems,[1,6] are therefore of interest for the full understanding of interactions involving open shell atoms. For O–He, there is substantial agreement on V_2 between present analysis and quantum chemical calculations.[16,22]

The interactions obtained in this work can be used in computation of macroscopic properties, such as the transport properties of oxygen atoms in rare gas baths.[23] Finally, information provided here should be valuable for a quantitative assessment of several phenomena, such as quenching by rare gases of metastable states of oxygen atoms[24] or emissions from rare gases oxide excimers[25] under various experimental conditions.

ACKNOWLEDGMENTS

This work has been supported by grants from the Italian Ministero della Pubblica Istruzione and from the Italian Consiglio Nazionale delle Ricerche.

[1]V. Aquilanti, E. Luzzatti, F. Pirani, and G. G. Volpi, J. Chem. Phys. **89**, 6165 (1988).
[2]V. Aquilanti and G. Grossi, J. Chem. Phys. **73**, 1165 (1980).
[3]V. Aquilanti, P. Casavecchia, G. Grossi, and A. Laganá, J. Chem. Phys. **73**, 1173 (1980).
[4]V. Aquilanti, G. Grossi, and A. Laganá, Nuovo Cimento. B **63**, 7 (1981).
[5](a) V. Aquilanti, G. Liuti, F. Pirani, F. Vecchiocattivi, and G. G. Volpi, J. Chem. Phys. **65**, 4751 (1976); (b) V. Aquilanti, E. Luzzatti, F. Pirani, and G. G. Volpi, *ibid.* **73**, 1181 (1980).
[6]V. Aquilanti, R. Candori, G. Liuti, L. Mariani, and F. Pirani, J. Phys. Chem. (in press).
[7](a) V. Aquilanti, G. Liuti, F. Vecchiocattivi, and G. G. Volpi, Mol. Phys. **21**, 1149 (1971); (b) V. Aquilanti, G. Liuti, F. Vecchiocattivi, and G. G. Volpi, Chem. Phys. Lett. **15**, 305 (1972); (c) F. Pirani and F. Vecchiocattivi, J. Chem. Phys. **66**, 372 (1977); (d) E. Luzzatti, F. Pirani, and F. Vecchiocattivi, Mol. Phys. **34**, 1279 (1977); (e) B. Brunetti, F. Pirani, F. Vecchiocattivi, and E. Luzzatti, Chem. Phys. Lett. **55**, 565 (1978); (f) **58**, 504 (1978); (g) B. Brunetti, R. Cambi, F. Pirani, F. Vecchiocattivi, and M. Tomassini, Chem. Phys. **42**, 397 (1979); (h) B. Brunetti, G. Liuti, E. Luzzatti, F. Pirani, and F. Vecchiocattivi, J. Chem. Phys. **74**, 6734 (1981).
[8]T. Nenner, H. Tien, and J. B. Fenn, J. Chem. Phys. **63**, 5439 (1975); **64**, 3902 (1976); see also Ref. 7(c).
[9](a) N. F. Ramsey, *Molecular Beams* (Clarendon, Oxford, 1956); (b) K. Berkling, Ch. Schlier, and P. Toschek, Z. Phys. **168**, 81 (1962); (c) M. A. D. Fluendy and K. P. Lawley, *Chemical Applications of Molecular Beams Scattering* (Chapman and Hall, London, 1973); (d) V. Aquilanti, F. Pirani, E. Luzzatti, and G. G. Volpi, Gazz. Chim. Ital. **110**, 57 (1980); (e) H. Hishinuma and O. Sueoka, Chem. Phys. Lett. **98**, 414 (1983); **121**, 293 (1985); (f) J. Reuss, *Atomic and Molecular Beams Methods*, edited by G. Scoles (Oxford, New York, 1987).
[10]B. Brunetti, G. Liuti, F. Pirani, and E. Luzzatti, Chem. Phys. Lett. **84**, 201 (1981).
[11]V. Aquilanti, G. Grossi, and F. Pirani, *Electronic and Atomic Collisions*, invited papers XIII ICPEAC, edited by J. Eichler, I. V. Hertel, and N. Stolterfoht (North Holland, Berlin, 1983), p. 441.
[12]V. Aquilanti, F. Pirani, and F. Vecchiocattivi, *Structure and Dynamics of Weakly Bound Molecular Complexes*, edited by A.Weber (Plenum, New York, 1987), p. 423.
[13]V. Aquilanti, E. Luzzatti, F. Pirani, and G. G. Volpi, Chem. Phys. Lett. **90**, 382 (1982).
[14]The beam direction is the natural collision quantization axis for the present experiments (see Sec. III). Therefore, states defined in the laboratory system with a quantization axis along the magnetic field direction have to be related to states in the collision frame with quantization axis along the beam direction by a suitable rotation matrix, corresponding to $\pi/2$ in the present arrangement [see also Refs. 1 and 5(b)].
[15]R. H. G. Reid and A. Dalgarno, Phys. Rev. Lett. **22**, 1029 (1969); R. H. G. Reid, J. Phys. B **6**, 2018 (1973).
[16]V. Aquilanti, R. Candori, E. Luzzatti, F. Pirani, and G. G. Volpi, J. Chem. Phys. **85**, 5377 (1986).
[17]F. Pirani and F. Vecchiocattivi, Mol. Phys. **45**, 1003 (1982).
[18]From H. J. Werner and W. Meyer, Phys. Rev. A **13**, 13 (1976), one has for the relative polarizability anisotropy of ground state oxygen atom, $(\alpha_\Sigma - \alpha_\Pi)/(\alpha_\Sigma + 2\alpha_\Pi) \simeq 0.18$. From the Slater–Kirkwood approximation [J. C. Slater and J. G. Kirkwood, Phys. Rev. **37**, 682 (1931)] this leads to $C_2/C_0 \simeq 0.22$, where C_2 is the long range R^{-6} anisotropic component [see Eq. (8)]. This value has been used for all systems.
[19]G. Liuti, E. Luzzatti, F. Pirani, and G. G. Volpi, Chem. Phys. Lett. **135**, 387 (1987).
[20]G. Liuti and F. Pirani, Chem. Phys. Lett. **122**, 245 (1985) and references therein. In that paper a general correlation was given in terms of atomic and molecular polarizabilities to obtain reasonable estimates of ϵ and R_m values for any interaction pair considered. These estimates agree within mutual uncertainties with present more refined MSV values.
[21]T. H. Dunning, Jr. and P. J. Hay, J. Chem. Phys. **66**, 3767 (1977); J. S. Cohen, W. R. Wadt, and P. J. Hay, *ibid.* **71**, 2955 (1979); S. R. Langhoff, *ibid.* **73**, 2379 (1980).
[22]V. Staemmler and R. Jaquet, Chem. Phys. **92**, 141 (1985).
[23]V. Aquilanti and F. Vecchiocattivi (to be published).
[24]D. L. Cunningham and K. C. Clark, J. Chem. Phys. **61**, 1118 (1974); P. S. Julienne, M. Krauss, and W. Stevens, Chem. Phys. Lett. **38**, 374 (1976); K. H. Welge and R. Atkinson, J. Chem. Phys. **64**, 531 (1976); J. Windrich, H. D. Wolf, and J. Fricke, J. Phys. B **11**, 1235 (1978); J. Bittner, K. Kohse-Höinghaus, U. Meyer, and Th. Just, Chem. Phys. Lett. **143**, 571 (1988).
[25]J. Goodman, J. C. Tully, V. E. Bondybey, and L. E. Brus, J. Chem. Phys. **66**, 4802 (1977); R. V. Taylor and W. C. Walker, J. Chem. Phys. **70**, 284 (1979); A. Kvaran, A. Ludviksson, W. S. Hartree, and J. P. Simons, Chem. Phys. Lett. **137**, 209 (1987).